DOI 10.1007/s11055-018-0701-6
Neuroscience and Behavioral Physiology, Vol. 49, No. 1, January, 2019

Methodological Features of the Morphometric Characterization of the Synaptoarchitectonics of the Human Neocortex by Immunofluorescent Detection of Neuromodulin

A. S. Stepanov, V. A. Akulinin, S. S. Stepanov, and D. B. Avdeev

UDC 611.813.1.018.86

Translated from Morfologiya, Vol. 153, No. 1, pp. 65–70, January–February, 2018. Original article submitted March 15, 2017. Revised version received October 6, 2017.

Objective. To study the possibility of using GAP-43 for morphometric characterization of synaptoarchitectonics. **Materials and methods.** Studies used immunofluorescent detection of neuromodulin (GAP-43) by confocal microscopy and automated computer image analysis of layer V (field 4) of the human brain (n = 4) using ImageJ 1.46. **Results.** Immunofluorescent detection of GAP-43 identified the distribution of axodendritic and axosomatic synapses, the total area of axon terminals, and the number densities of intermediate and large terminals. **Conclusions.** A necessary condition for obtaining accurate data is having digital images with sufficient resolution (600–900 pixels per inch). These results need to be considered in studies of the synaptoarchitectonics of the neocortex using immunohistochemical methods for investigating synapse structure.

Keywords: neocortex, synapses, neuromodulin, immunofluorescence, automated computer analysis.

Because of the small sizes of synaptic contacts (0.1–0.5 μm) and the terminal branches of axons (about 1–3 μm), most scientific information on these structures has ben obtained by electron microscopy (EM) [4, 5, 10, 11]. However, it is difficult to obtain qualitative and quantitative characteristic of synapse distribution within large anatomical brain formations (such as the neocortex) using EM. Light and immunofluorescence microscopy easily cope with this task [1, 2, 3, 6]. Immunohistochemical reactions for synaptophysin (p38) and neuromodulin (GAP-43) are widely used for this purpose [1].

The reaction for p38 allows the locations of synaptic vesicles (SV) of diameter 50 nm to be identified. This protein is a member of the family of integral SV membrane-bound proteins, occupies 10% of their volume, and is present in all synapses [7, 9]. The reaction for GAP-43 provides data on the structural-functional sate of axosomatic and axodendritic synaptic terminals. This is because GAP-43 phosphoprotein is specific for the membranes of axon terminals as a growth marker. The presence of GAP-43 expression in nervous tissue is a sign of the onset of axon formation in embryogenesis; it takes an active role in nervous tissue regeneration and plasticity processes [8, 12].

The possibility of morphometric characterization of synapses in the human neocortex by immunohistochemical detection of synaptophysin, i.e., SV, has been studied previously [2]. However, SV constitute a subsystem of the synaptic terminal and largely characterize its vesicular pool. Furthermore, SV are very variable structures and undergo the light type of destruction at the early stages of the postischemic period, when synaptic terminals are still relatively well preserved [4]. There is therefore value in studying the possibility of morphometric characterization of synaptoarchitectonics by immunohistochemical detection of GAP-43, and this was the aim of the present work.

Studies were performed at Omsk State Medical University. Material for histological studies was obtained at Omsk District Forensic Medical Office. The study was approved by the Omsk State Medical University Ethics Committee (protocol No. 61 of June 19, 2014).

Department of Histology, Cytology, and Embryology, Omsk State Medical University, Ministry of Health of the Russian Federation, Omsk, Russia;
e-mail: ctepan55@yandex.ru, akulinin@omsk-osma.ru.

TABLE 1. Relationship between Morphometric Parameters of Mask Particles (n = 50) of Neuropil Images and Its Final Resolution (field of view size 384 × 256 μm)

Field of view parameter	Resolution of final image, pixels/inch			
	72	300	600	900
Number of particles, absolute number	929 ± 155	1439 ± 206 $p < 0.001$*	2216 ± 330 $p < 0.001$*	2650 ± 450 $p < 0.001$*
Area of all particles, pixels	1598 ± 340	32291 ± 6558	180690 ± 36138	523333 ± 104666
Mean particle size, μm^2	1.72 ± 0.3	1.31 ± 0.2 $p < 0.001$*	1.14 ± 0.2 $p = 0.001$*	1.18 ± 0.3
Smallest particle size, μm^2	1.0	0.058 $p < 0.001$*	0.014 $p < 0.001$*	0.012
Relative area of all particles, %	1.54 ± 0.4	1.85 ± 0.6 $p = 0.004$*	2.58 ± 0.4 $p < 0.001$*	3.36 ± 0.6 $p < 0.001$*
Total number density of terminals per 100 μm^2 of neuropil	1.0 ± 0.2	1.5 ± 0.5 $p < 0.001$*	2.3 ± 0.6 $p < 0.001$*	2.7 ± 0.5 $p < 0.001$*

*Statistically significant differences compared with previous value (Student's t test for linked sets).

Studies used autopsy materials (collected 5–10 h after death) from Brodmann field 4 of the cerebral cortex (CC) from people dying in accidents (n = 4: men aged 23–45 years).

Brains were fixed in 4% paraform in 0.1 M phosphate buffer pH 7.2–7.4 at 4°C for one day and embedded in paraffin. Serial frontal sections of thickness 10 μm were cut through all layers and were mounted on slides. Fluorescence microscopy used primary polyclonal rabbit antibodies (IgG) to neuromodulin (GAP-43). Immune reactions were visualized using goat polyclonal secondary antibodies to rabbit immunoglobulin (Abcam, England) (diluted 1:200). Antibodies were conjugated with the fluorescent dye Texas Red® sulfonyl chloride (Abcam, England).

Preparations were examined using a confocal laser scanning microscope attached to a Bio-Rad MRC 600 CLSM Nikon FXA fluorescence microscope (Nikon, Japan). An argon-krypton laser was used with filters for fluorescein isothiocyanate (488DF-10) and lipofucsin (568DF-10). Two-channel fluorescence (lens magnification ×20, Nikon objective; Fluor 1.30) was used with an image examination step of 2 μm, field magnification ×3, mean density 1. A rapid examination regime was used (10 examinations of each section) using Calman filters with a coefficient of 3 and a block size of ¼, with data storage in computer memory. The matrix scanning unit (pixel) size was 0.49 × 0.49 μm.

Immunofluorescence and lipofucsin fluorescence were initially recorded using a 488DF-10 filter though channel 1 (green) with image capture of 5–10 Z-series sections, followed by examination of the same area to detect lipofucsin with a 568DF-10 filter through channel 2 (red). Image files were formed and ImageJ 1.46 was used to analyze images of labeled synapses.

Statistical hypotheses were tested using Statistica 8.0 to run the nonparametric Mann–Whitney U test and the Kolmogorov–Smirnov test for pairwise comparisons and the χ^2 test for relative values. Null hypotheses were rejected at statistical significance $p < 0.05$. Morphometric analysis determined the following characteristics: number and area of particles in the field of view, mean and smallest sizes, relative areas, and total number densities (TND) of terminals.

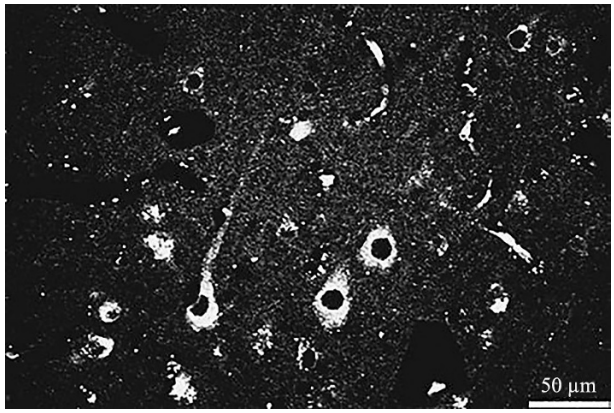

Fig. 1. GAP-43-positive structures in layer V of the motor area of the human CC (field 4). Fluorescent immunohistochemical reaction.

Studies of layer V of the neocortex showed that GAP-43 immunofluorescence reactions labeled small, intermediate, and large structures in the neuropil and on neuron bodies (Fig. 1).

Neurons with intense discrete staining of GAP-positive material over the whole perikaryon surface dominated. The neuropil of the neocortex contained numerous clear granules of immunohistochemical reaction product, mostly round in shape. GAP-43-positive structures in the neuropil were distributed nonuniformly as intensely fluorescing granules (see Fig. 1).

At the first stage of automatic analysis, the size and shape of particles on image masks were not limited. This

TABLE 2. Distribution of Area Sizes of Particles Identified in Masks for One Field of View of the Neuropil

Resolution, pixels/inch	Particle area, μm²	Number of particles	
		abs. number	%
72	<1.0	0	0
	1.0–1.7	631	67.9
	1.8–3.0	226	24.4
	3.1–4.6	28	3.0
	>4.6	44	4.7
300	0.2–0.9	783	54.4
	1–2.4	478	33.2
	2.5–4.0	114	7.9
	>4.0	63	4.5
Friedman ANOVA	df = 3; $\chi^2 = 55.1$; $p < 0.0001$*		
600	0.02–0.96	1233	55.6
	1–2.8	802	36.2
	2.9–4.8	121	5.5
	>4.8	59	2.7
Friedman ANOVA	df = 3; $\chi^2 = 18.4$; $p = 0.0004$*		
900	0.01–0.96	1459	55.1
	1–2.8	988	37.3
	2.9–4.8	154	5.8
	>4.8	49	1.8
Friedman ANOVA	df = 3; $\chi^2 = 4.3$; $p = 0.2$		

*Statistically significant differences in structure of particle distribution compared with previous final image resolution, $p < 0.05$ (χ^2 test).

allowed all components of real images to reflect GAP-43-positive structures. Thus, in Fig. 2, all such structures (terminals of axosomatic and axodendritic synapses), depending on the final image resolution, occupied 6.4% (resolution 72 pixels/inch), 6.9% (300 pixels/inch), 9.5% (600 pixels/inch), and 13.7% (900 pixels/inch) of the field of view.

At the second stage, only round particles reflecting GAP-43-positive structures in the neuropil were detected (terminals of axospinous and axodendritic synapses) (see Fig. 2, *b*). Neuropil structures occupied 1.6% (resolution 72 pixels/inch), 1.9% (300 pixels/inch), 2.6% (600 pixels/inch), and 3.4% (900 pixels/inch) of the field of view (98304 μm²).

Thus, the number and area of particles of different sizes and shapes in the mask of real images of the neuropil depended on the final resolution (72, 300, 600, or 900 pixels/inch). The highest values for total area and number density of particles in the neuropil were obtained at resolutions of 600 and 900 pixels/inch (Table 1).

Thus, fluorescence immunohistochemical detection of neuromodulin using a confocal microscope and high (600–900 pixels/inch) final digital image resolution led to the detection of fluorescing particles of size less than 1 μm² (≥0.02 μm²) in the neocortical neuropil. However, these particles accounted for no more than 2.5% of the total detected. Most fluorescing structures were particles of size 0.1–0.3 μm², so probably terminals or conglomerates of terminals with diameters of 0.4–2.0 μm.

Using a final resolution of 900 pixels/inch, TND of terminals in the neuropil in the CC was 2.7 ± 0.5 per 100 μm²; these terminals occupied 35.8% of the total area of GAP-positive material. The remaining area (64.2%) was occupied by terminals on perikarya and large dendrites. Immunofluorescent detection with GAP-43 identified the population of very small (<0.1 μm²) terminals only partially (10–20%). This is very probably associated with the insufficient energy of the fluorescing molecules and the low resolution of the microscope. In addition, examination of sections with a step

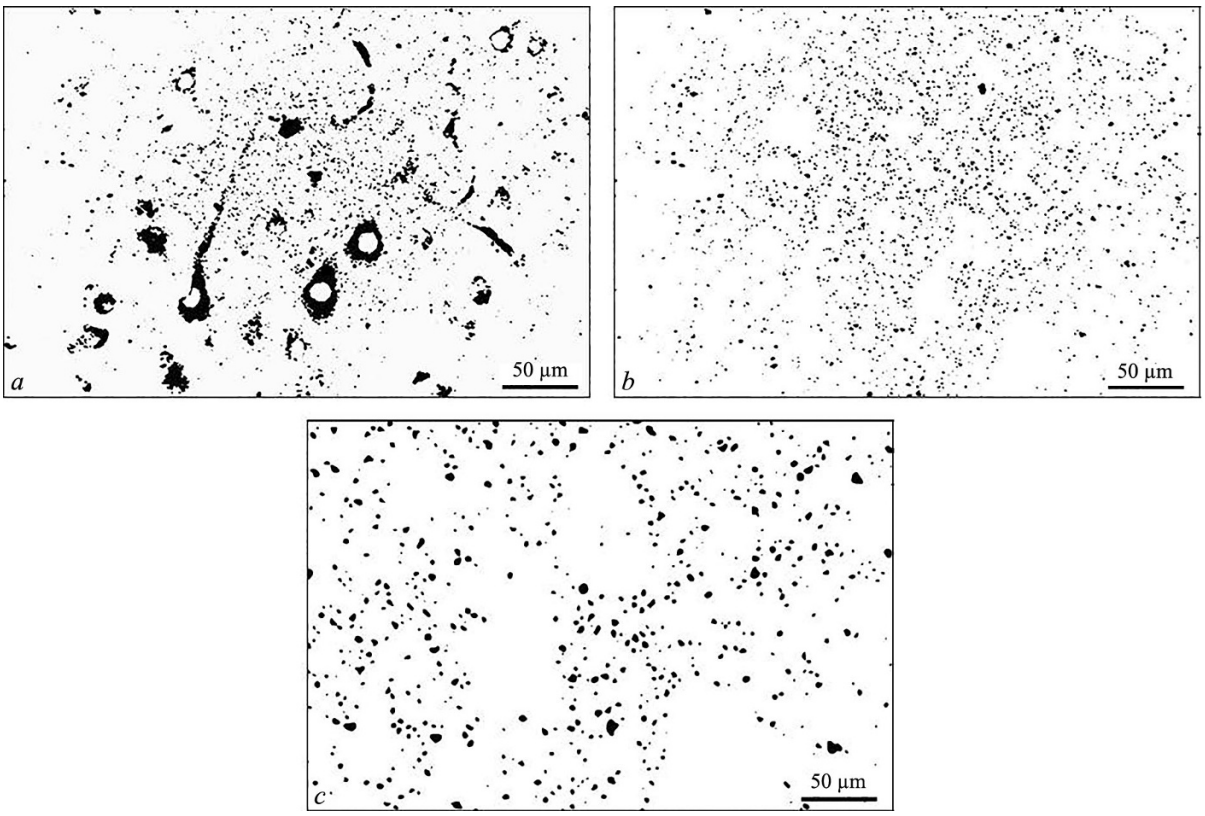

Fig. 2. Mask and images of field of view of layer V of the human cerebral cortex created by ImageJ 1.46 (original in Fig. 1). *a*) All GAP-43-positive structures; *b*) only structures of the neuropil; *c*) magnified fragment. Arrows show locations of cell bodies.

of 2 μm showed that some terminals simply overlapped each other and could not be identified individually.

An increase in the resolution of the final image from 72 to 900 pixels/inch provided for more precise assessment of the TND of terminals – from 929 to 2650 per field of view (a 2.85-fold increase). The relative area of the particles identified increased, not directly proportionally, from 1.6% to 3.4% (a 2.13-fold increase) (see Table 1).

The distribution by area of particles (individual terminals and groups) identified on masks of real images of the neuropil is shown in Table 2. At a starting final image resolution of 72 pixels/inch, terminals of area <1.0 μm^2 were not detected, but were probably counted as parts of larger particles. Increases in resolution to 300, 600, and 900 pixels/inch led to increased detail in the image and statistically significant increases in the numbers of small particles, accompanied by a reduction in the proportion of large particles (see Table 2).

The difficulty of studying axosomatic synapses is that GAP-43-positive structures making up terminals on the perikarya of most neurons fused into fluorescing unstructured conglomerates with high brightness (Fig. 3, *a*, *b*).

It is difficult to identify the sizes and shapes of the structures forming these conglomerates using automated analysis. To solve this, areas of perikarya on which individual round-shaped particles were visible were highlighted manually. This was followed by morphometric analysis (see Fig. 3, *a*).

The smallest area of individual particles on neuron perikarya was 0.40 μm^2 (diameter 0.7 μm), the mean area was 2.40 μm^2 (diameter 1.75 μm), and the greatest was 4.20 μm^2 (diameter 2.30 μm). The most common were round terminals of area 1.50–2.20 μm^2. These formed larger and unevenly shaped conglomerates, partially or completely covering nerve cell bodies (see Fig. 3, *a*, *b*).

TND of axon terminals per unit area of pyramidal neuron perikaryon (in conglomerates) was 103 ± 33/100 μm^2, while the value in the initial segments of apical dendrites was only 14.2 ± 4.4/100 μm^2. Overall, axosomatic and axodendritic synapses on large dendrites (based on examination of 50 fields of view) was 49.7–77.5% (95% confidence interval) of the total area of GAP-43-positive structures in layer V of the neocortex in normal conditions, all others accounting for 22.7–50.6%. a pattern was found: the further from the neuron body, the lower the TND of terminals per unit area/volume of component (body 103 ± 33/100, large dendrites 14.2 ± 4.4, neuropil 2.7 ± 0.5/100 μm^2). Receptive field areas in the main compartments of neurons were discriminated less significantly. This is evidence that synapses located on the perikaryon and large dendrites, because of

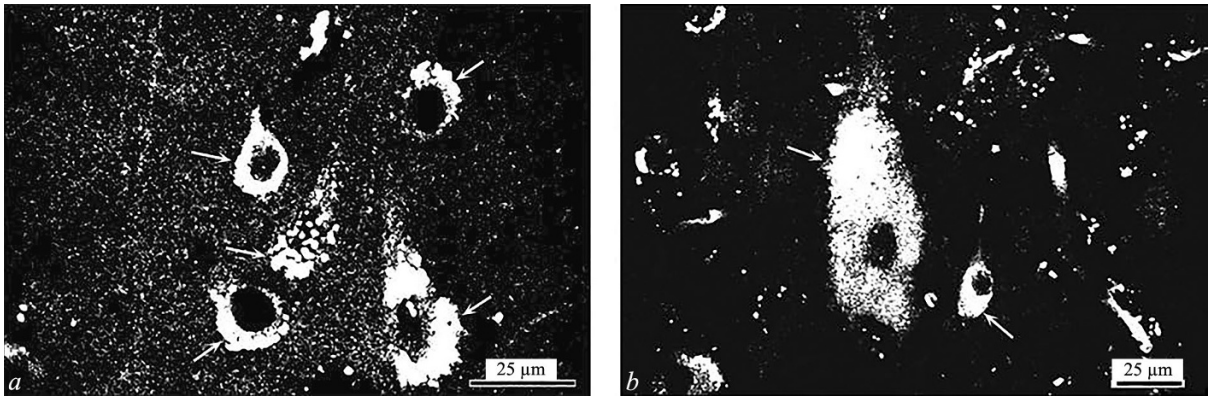

Fig. 3. GAP-43-positive structures on neuron bodies and dendrites (arrows) in layer V of the human cerebral cortex (field 4). *a*) Neuron of intermediate size; *b*) large and small neuron. Fluorescent immunohistochemical reaction.

their greater density, had more information content and more influence on pyramidal neurons than axospinous synapses.

Thus, immunofluorescence studies of GAP-43 can yield objective information on the disposition and areas of axospinous, axodendritic, and axosomatic synapses. However, there are limitations in determining the number density of small terminals (<1 μm^2). This is probably linked with the insufficient fluorescence intensity of small groupings of fluorescing molecules, the relatively low resolution of the microscope and digital camera sensor, fusion of images of neighboring brightly fluorescing terminals in terms of homogeneous conglomerates, and the vertical superimposition of terminals at different scanning levels [1–3].

This problem was partially solved by increasing the resolution of the final image to 600–900 pixels/inch. However, only 10–20% of the smallest terminals (<0.01 μm^2) were seen at this resolution. As a result, the TND of terminals (labeled with GAP-43-particles) in the neuropil (where small synapses are located) was lower (2.7 ± 0.5/100 μm^2) than seen by EM (15–18/100 μm^2). This approach has previously been used in studies of synapses in layer III of the frontal CC in humans using immunohistochemical detection of synaptophysin [2]. The authors were able to determine the TND of synapses at the level of 1.0/100 μm^2, which is close to our results.

An additional methodological challenge was associated with detection of individual terminals in large, intensely fluorescing conglomerates of GAP-43-positive structures on perikarya. Possible solutions to this problem were to reduce the thickness of scan sections or to apply morphometry to the peripheral zones of conglomerates in which individual terminals were visible. In terms of size, these terminals showed a very high density of axosomatic synapses on pyramidal neurons in the motor CC in humans – 103 ± 33/100 μm^2. The high total numerical density of axosomatic synapses is also evidenced by published data [10, 11].

Our results need to be considered in investigations of the synaptoarchitectonics of the neocortex using immunohistochemical methods for assessing synapse structure. These methods can yield accurate objective data on the contents of synaptic proteins in large volumes of nervous tissue and allow synapses to be detected on neuron perikarya and dendrites. However, detailed study of the number density and distribution of small synapses requires additional methods (reconstruction from serial sections, electron and high-resolution fluorescent microscopy).

Authors' contributions. Study concept and design: A.S.S., V.A.A., S.S.S., D.B.A.; collection and processing of material: A.S.S., D.B.A.; statistical analysis of data: A.S.S., V.A.A., S.S.S., D.B.A.; writing: A.S.S., V.A.A., S.S.S., D.B.A.

The authors have no conflicts of interests.

REFERENCES

1. E. G. Gilerovich, E. G. Sukhorukova, O. V. Kirik, I. P. Grigor'ev, and D. E. Korzhevskii, "Detection of specialized synaptic groups (glomeruli) in the human cerebellum using an immunocytochemical reaction for synaptophysin and confocal laser microscopy," *Morfologiya*, **146**, No. 5, 73–77 (2014).
2. A. V. Mytsik, V. A. Akulinin, S. S. Stepanov, and P. M. Larionov, "Potential for morphometric characterization of human neocortex synapses in immunohistochemnical verification," *Sibirsk. Med. Zh.*, **118**, No. 3, 66–69 (2013).
3. A. V. Mytsik, V. A. Akulinin, S. S. Stepanov, A. V. Sergeev, and P. M. Larionov, "Immunofluorescence verification and morphometry of axosomatic synapses in the human neocortex in acute and chronic ischemia," *Morfol. Ved.*, No. 3, 53–60 (2012).
4. V. V. Semchenko, S. S. Stepanov, and N. N. Bogolepov, *Synaptic Plasticity of the Brain (basic and applied aspects)*, Media-Sfera, Moscow (2014), 2nd ed.
5. V. V. Semchenko, S. S. Stepanov, and S. I. Ereniev, "Structural-functional recovery of nervous tissue in the brain during the postischemic period from the point of view of the concept of the provisional nature of repair histogenesis," *Tikhookeansk. Med. Zh.*, No. 2, 98–102 (2016).
6. A. V. Sergeev, S. S. Stepanov, V. A. Akulinin, and A. V. Mytsik, "Natural protective mechanisms of the human brain in chronic ischemia," *Obshsh. Reanimatol.*, **11**, No. 1, 22–32 (2015).
7. C. P. Arthur and M. H. B. Stowell, "Structure of synaptophysin: a hexameric MARVEL-domain channel protein," *Structure*, **15**, No. 6, 707–714 (2007), doi: 10.1016/j.str.2007.04.0118.

8. G. Grasselli and P. Strata, "Structural plasticity of climbing fibers and the growth-associated protein GAP-43," *Front. Neural. Circuits*, **7**, No. 25, 1–7 (2013), doi: 10.3389/fncir.2013.000259.
9. S. E. Kwon and E. R. Chapman, "Synaptophysin regulates the kinetics of synaptic vesicle endocytosis in central neurons," *Neuron*, **70**, No. 5, 847–854 (2011), doi: 10.1016/j.neuron.2011.04.00110.
10. J. I. Luebke, M. Medalla, J. M. Amatrudo, C. M. Weaver, J. L. Crimins, B. Hunt, P. R. Hof, and A. Peters, "Age-related changes to layer 3 pyramidal cells in the rhesus monkey visual cortex," *Vis. Cereb. Cortex*, **25**, No. 6, 1454–1468 (2015), doi:10.1093/cercor/bht33611.
11. A. Peters, C. Sethares, and J. I. Luebke, "Synapses are lost during aging in the primate prefrontal cortex," *Neuroscience*, **152**, No. 4, 970–981 (2008), doi: 10.1016/j.neuroscience.2007.07.01412.
12. S. M. Powell, "Gene targeting of presynaptic proteins in synaptic plasticity and memory: across the great divide," *Neurobiol. Learn. Mem.*, **85**, No. 1, 2–15 (2006), doi: 10.1016/j.nlm.2005.08.014.